A Parallel, High-Fidelity Radar Model

Matthew Horsley, Benjamin Fasenfest
Lawrence Livermore National Laboratory

ABSTRACT

Accurate modeling of Space Surveillance sensors is necessary for a variety of applications. Accurate models can be used to perform trade studies on sensor designs, locations, and scheduling. In addition, they can be used to predict system-level performance of the Space Surveillance Network to a collision or satellite break-up event.
A high fidelity physics-based radar simulator has been developed for Space Surveillance applications. This simulator is designed in a modular fashion, where each module describes a particular physical process or radar function (radio wave propagation & scattering, waveform generation, noise sources, etc.) involved in simulating the radar and its environment. For each of these modules, multiple versions are available in order to meet the end-users needs and requirements. For instance, the radar simulator supports different atmospheric models in order to facilitate different methods of simulating refraction of the radar beam. The radar model also has the capability to use highly accurate radar cross sections generated by the method of moments, accelerated by the fast multipole method. To accelerate this computationally expensive model, it is parallelized using MPI.
As a testing framework for the radar model, it is incorporated into the Testbed Environment for Space Situational Awareness (TESSA). TESSA is based on a flexible, scalable architecture, designed to exploit high-performance computing resources and allow physics-based simulation of the SSA enterprise. In addition to the radar models, TESSA includes hydrodynamic models of satellite intercept and debris generation, orbital propagation algorithms, optical brightness calculations, optical system models, object detection algorithms, orbit determination algorithms, simulation analysis and visualization tools. Within this framework, observations and tracks generated by the new radar model are compared to results from a phenomenological radar model. In particular, the new model will be used to simulate an S-band upgrade to the space fence.

1. INTRODUCTION

Computer models of radars in the Space Surveillance Network can be a useful tool for evaluating new sensor locations, designs, and operational parameters. Such models can also be used to study tasking algorithms and predict the system performance to new debris. However, when performing many trade studies or simulations spanning several simulated days, these models can have unacceptable run times. This leads to a trade-off between the inclusion of all relevant physics in the model and simulation time. This paper details a radar model which answers the run-time problem while maintaining a high level of modeling fidelity by using parallelization. The radar model, which is implemented in Lawrence Livermore National Laboratory's TESSA (Testbed Environment for Space Situational Awareness) is designed to run on Linux cluster supercomputers. It utilizes a modular framework which allows different physics models to be used as appropriate for any radar. This general nature makes it a good tool for modeling many different sensors with the same software. Highly accurate modules have been created for noise sources, antenna effects, atmospheric effects on propagation, and the radar cross sections of targets. These modules are combined in a framework which uses parallelization to divide the simulation work load on a pulse-by-pulse basis with each processor being responsible for all computations involving a single pulse. This paper will first describe several of the physics modules in the simulation, then explain the parallelization scheme and present an example simulation with timing results.

2. RADAR MODELING

2.1 EXTERNAL NOISE SOURCES

One of the fundamental quantities that a radar can measure with its antenna is the radiation power per unit area, per unit frequency. In the microwave regime, this is usually given the name brightness temperature, T_b. There are various sources which contribute to the brightness temperature. They include external sources outside of the earth's atmosphere (e.g. cosmic or galactic noise), emission from atmospheric gases, and emission and scattering from the ground. This section will deal with modeling cosmic contributions to the brightness temperature,

[1]This work performed under the auspices of the U.S. Department of Energy by Lawrence Livermore National Laboratory under Contract DE-AC52-07NA27344. UCRL # LLNL-CONF-454075

$T_{ext} = T_{CMB} + T_{gal}$. T_{CMB} is the temperature due to the cosmic microwave background emission and is usually modeled as a constant, 2.73 K. A common way to model the galactic noise, T_{gal}, is to use a well defined median temperature at a reference frequency, and apply a scaling law to model the galactic noise temperature at a different frequency, as is shown in eqn. 2.1.1.

$$T_{gal}(f) = T_{ref}\left(\frac{f_{ref}}{f}\right)^{\beta} \qquad (2.1.1)$$

Typical values for the parameters in equation 2.1.1 are: $T_{ref} = 20\ K$, $\beta = 2.75$, and $f_{ref} = 408\ MHz$. This method is very computationally efficient, but effectively averages over any variations in temperature due to galactic structure, bright point sources, etc… In [1], a method for computing the sky temperature is provided that models the angular distribution of the galactic noise sources and covers a wide range of frequencies from 10 MHz to 300 GHz. The model is based on a numerical fit to a radio emissions data set derived from all publically available total power, large-area radio surveys. The inputs to the galactic nosie model include the radar's operating frequency, location, year, month and day, and time. The outputs are contained in a table of temperatures indexed with galactic latitude and longitde. A routine to convert from galactic longitude and latitude is used to translate the results to the radar's coordinate system. Using this method allows a detailed model of the angular distribution of the galactic noise as measured by a particular radar at any location, date, time of day and operating frequency. An example of this is shown below in Figure 1, for a radar located at Death Valley, CA at night time, operating at a frequency of 408 MHz. Galactic radio emissions can be a significant source of noise for frequencies below ~1 GHz, but rapidily become neglibible for frequencies much beyond this (see fig. 1, right panel). Future work in this area will focus on modeling man-made sources of RF noise and scattering from the ground.

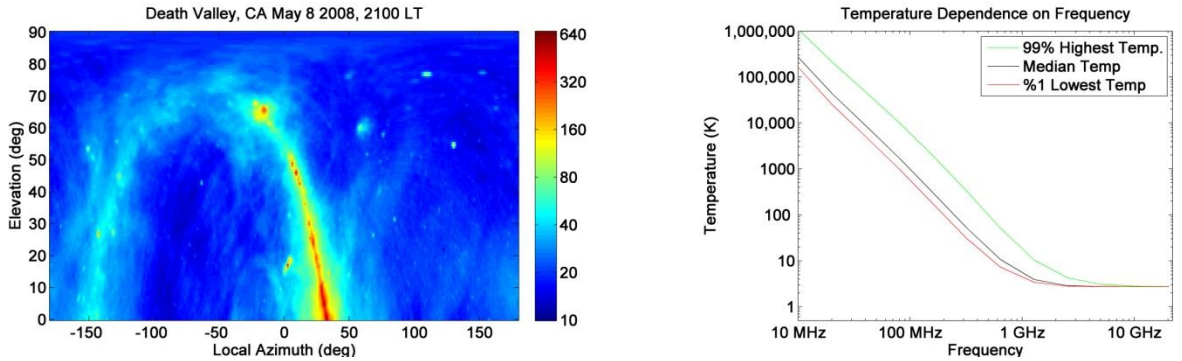

Figure 1 (Left Panel) Simulated galactic noise distribution at 408 MHz for a location in Death Valley. (Right Panel) The galactic noise temp. dependence with frequency, taken over all gal. latitudes and longitudes.

2.2 ATMOSPHERIC MODELS

This section will describe the different atmosphere models that are currently available in the simulation framework. The Earth's atmosphere can affect the propagation of Radio Frequency (RF) energy in a number of different ways, e.g. refractive bending, attenuation, range-delay, Doppler frequency shifts, polarization rotation, frequency spreading and rapid amplitude and phase scintillation [2]. Accurately modeling these effects is a critical step in the simulation, as it affects the quality of the measurements generated by the radar which are used in computing orbital parameters of objects being tracked by the radar. In order to support simulation activities that require a high level of accuracy in the modeling, we have incorporated high fidelity models of the atmosphere into the simulation (when available). Lower fidelity models are also included in the simulation, which are useful for conducting a large number of simulations very quickly. The inputs to the different models can include geographical latitude, longitude, altitude, time and date. The outputs for the neutral atmosphere models are altitude dependent temperature, pressure and water vapor pressure. The output for the ionosphere model is the electron density as a function of the model parameters. The simulated atmosphere is then used in modeling the effect of the atmosphere on the propagation of the RF energy.

Currently, there are 7 neutral atmospheric models and 2 ionospheric models available for use within the simulation framework. The first type of neutral atmosphere model available to the simulation user is an exponential approximation to the neutral atmosphere, see [3] for details. The second class of neutral atmosphere model includes a set of Standard Atmospheres [4]. A "Standard Atmosphere" is defined as a vertical distribution of atmospheric

parameters that are representative of Earth's atmosphere. There are 6 types of Standard Atmospheres in the simulation framework; US Standard, Tropical, Mid-latitude (summer and winter), and Sub-Arctic (summer and winter). Each standard atmosphere makes use of a data base that provides realistic vertical profiles of atmospheric temperature, pressure, water content and gas mixing ratios from ground level to an altitude of 120 km. These parameters are used in computing the index of refraction for modeling propagation effects in the neutral atmosphere; see section 2.3 for more details.

Two different models of the ionosphere are available to the simulation user. The first [5] approach is a phenomenological model of the ionosphere that captures large scale variations in the electron density as a function of altitude. The second ionosphere model available to the user is the International Reference Ionosphere (IRI) [6]. The IRI modeling effort was started in 1969 and has been steadily improved on each year. This provides a higher fidelity estimate of the electron density as a function of a large number of variables. Typical runs will execute the IRI routines using the radar's position, simulation date and the time of day with all other IRI variables to their default values. An example of the IRI model output is shown in Figure 2. In the left panel the Total Electron Content (TEC) is plotted as a function of latitude and longitude. In the right panel, range delays due to the ionosphere are plotted as a function of frequency. For operating frequencies above a few GHz, ionospheric effects are typically not important and can be readily corrected for by the radar. For operating frequencies much below 1 GHz, ionospheric effects become more pronounced and will require the radar to perform a dual frequency correction or employ sophisticated single frequency correction schemes. These sorts of corrections performed by the radar are not currently modeled in the simulation and will be a focus for future development work. In addition to modeling the corrections performed by the radar, future work will focus on incorporating Numerical Weather Models into the simulation framework. This will enable a more realistic model of the day-to-day (and even hour-to-hour) changes in the atmospheric conditions that affect the operations of the radar.

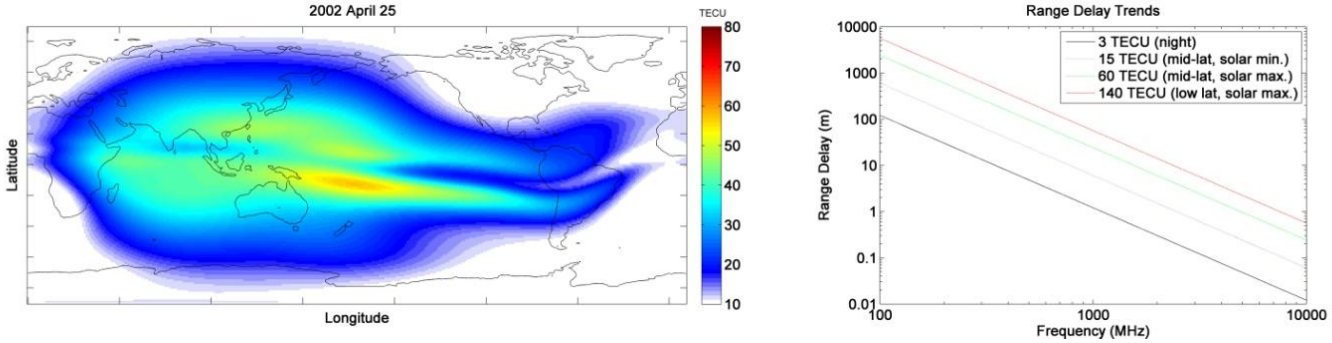

Figure 2 (Right panel) Ionospheric TEC as a function of latitude and longitude for April 25, 2002, UT = 5 hours. (Left panel) Ionospheric range delay as a function of frequency for a number of different conditions.

2.3 RF PROPAGATION EFFECTS

The atmospheric conditions are simulated for a given radar's location, current time, day, month and year using one of the models described in section 2.2. The temperature, pressure, water vapor pressure and electron density obtained from the atmosphere model are used to compute a 3 dimensional, complex refractivity map of the sky as viewed from the radar's position. This refractivity map is then used with a ray-tracing procedure to compute the path taken by the RF ray as it travels through the atmosphere. Once the path has been computed, the amount of refraction that occurred is known, the range delay can be computed and the total attenuation suffered by the ray can be calculated by integrating the specific attenuation along the ray's path. The atmospheric attenuation will affect the measured Radar Cross Section (RCS) and the signal-to-noise ratio. The range delay and refractive bending will affect the measurement's range and angular accuracies.

Liebe's Millimeter-wave Propagation Model (MPM) [7] is used to model the complex refractivity in the neutral atmosphere for frequencies up to 1000 GHz. The complex refractivity, $N_t(f)$, as defined by Leibe is composed of three parts, a nondispersive component N_0 which is real and positive, along with a set of real $N(f)'$ and imaginary $N(f)''$ components,

$$N(f)_t = N_0 + N(f)' - jN(f)'' \qquad ppm.$$

The imaginary component is related to power attenuation through the following expression,

$$\alpha = 0.1820\ f\ N''(f) \qquad dB/km$$

and the real part describe phase dispersion,

$$\beta = 1.2008\ f\ N'(f) \qquad deg/km\ ,$$

where f is the frequency in GHz. An example of how the index of refraction is used in the code base is shown in figure 3. The left panel show a comparison of the refractive bending in the neutral atmosphere as a function of the initial elevation angle. Significant bending occurs for low elevations and moist atmospheres (Tropical). The middle panel shows the index of refraction in the neutral atmosphere as a function of altitude. Variations in the refractive index due to different atmospheric conditions are limited to the first ~30 kilometers of the earth's surface. The ray tracing routine was validated using a number of different cases. The left panel shows the refractive bending in an exponential atmosphere as computed using the ray trace routine (black asterisk) and an analytical approximation (black line) [8], showing excellent agreement. Another example of the ray trace validation is show in the rightmost panel. A simulation of a Maxwell's Eye refractive medium was performed (grayscale indicates index of refraction) and a number of different rays were traced. The comparison between the numerical results and theoretical expectations agreed to within 0.001% for this simple case.

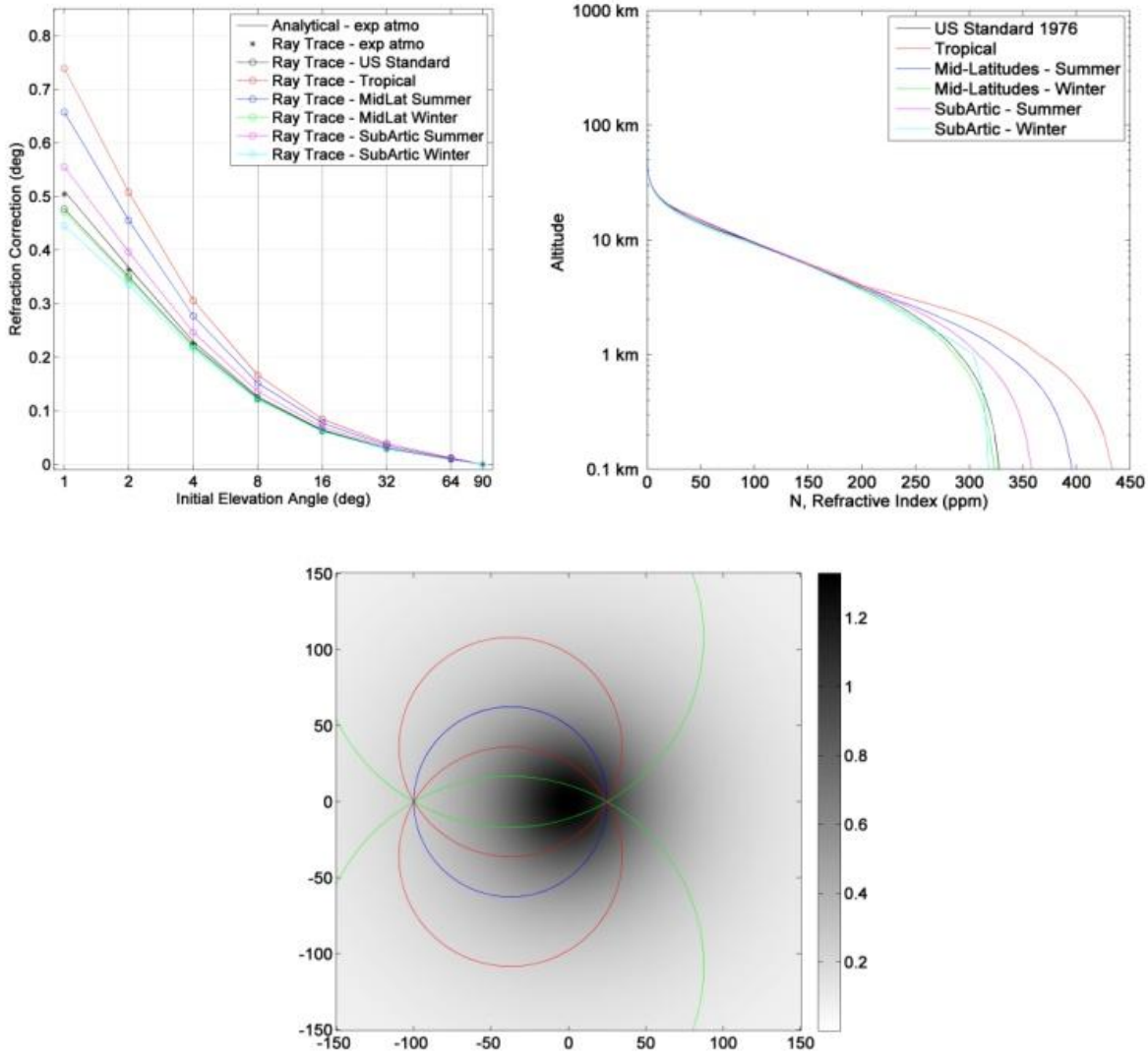

Figure 3. (Top Left) A comparison of the elevation dependent refractive bending for a number of different cases. (Top Right) Index of refraction as a function of altitude. (Bottom) An example of a Ray Trace validation case.

The Appleton-Hartree equation (see [9]) serves as the starting point for modeling the index of refraction in the ionosphere,

$$n^2 = 1 - \frac{X}{U - \frac{Y^2 \sin^2\theta}{2(U-X)} \pm \left(\frac{Y^4 \sin^4\theta}{4(U-X)^2} + Y^2 \cos^2\theta\right)^{1/2}},$$

where $X = \omega_p^2/\omega^2$, $Y = \mu_0 He/m\omega$, $U = 1 - jv/\omega$, and $\omega_p = \sqrt{Ne^2/\varepsilon_0 m}$. The angular plasma frequency is ω_p, N is the electron density, e and m are the charge and mass of an electron, ε_0, μ_0 are the electric and magnetic permittivity of free space, H is the geomagnetic field intensity, v is the collision frequency, θ is the angle made between the wave normal and the geomagnetic field, and the $\pm$ refers to the ordinary and extra-ordinary waves. As described in [9], a simplification can be made for frequencies above VHF, yielding the expression

$$n \approx 1 - \frac{1}{2}X = 1 - b\frac{N}{\omega^2},$$

where $b = e^2/2\varepsilon_0 m$. This approximation ignores the effect of the splitting of the ordinary and extra-ordinary waves and thus reduces the index of refraction to a function solely based on the electron density, radar operating frequency, and a few physical constants. The electron density can be simulated using the ionosphere models described in sec. 2.2.2 and will be a function of year, month, day, time of day , geographic latitude, longitude and altitude

Since the earth's atmosphere emits and absorbs RF energy, we use Radiative Transfer Theory to model the noise power measured with the radar antenna, T_b. Following [10], the noise power can be related to the galactic brightness temperature T_{gal}, and the atmospheric temperature T.

$$T_b = T_{gal}\, e^{-\tau(0,L)} + \int_0^L \alpha(x')T(x')\, e^{-\tau(0,x')}\, dx',$$

where $\tau(x', x) = \int_{x'}^{x} \alpha(s)\, ds$ is the optical thickness and $T(x')$ is the temperature of the atmosphere at an altitude x'. The ray trace routine is used within the integration routine. By ignoring scattering effects we limit ourselves to cases without significant rain, smoke, and other scattering sources. An example of the effects of radiative transfer theory has on the noise power measured by the radar is shown in figure 4 below.

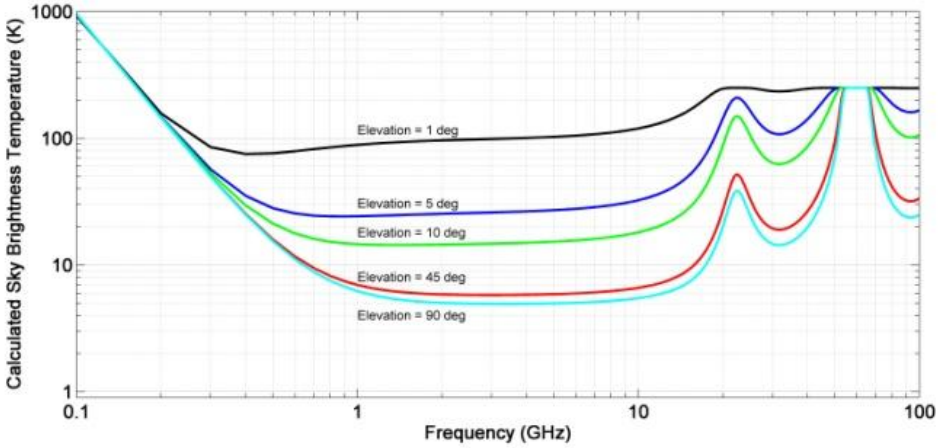

Figure 4. Example of a Radiative Transfer Theory calculation for a number of different elevation angles.

2.4 ANTENNA EFFECTS

The radar antenna is used to transmit and receive RF energy, and can have many different designs and capabilities. Currently, the simulation supports rectangular, phased array antennas. The option of using a dish antenna will be incorporated into the simulation as part of future work. The phased array antenna is defined in the simulation by a number of variables; (1) type of radiator, (2)the number of radiators along the width and length of the antenna, (3) the spacing of the radiators, (4) orientation of radiators, (5) the number of bits used in the phase shifters, (6) the location of the antenna, (7) orientation of antenna, (8) antenna efficiency, and (9) the drift rate of Inertial Measurement Unit (IMU).

The user can select from two pre-defined radiating elements (half-wave, Hertzian dipole). If desired, the option of a user-defined radiating element (such as a waveguide, horn, etc…) is supported by the simulation as well. The user has the option of switching on a model of a strap-down IMU co-located with the radar antenna. This will allow a

simulation of the performance degradations due to imperfect motion compensation, errors in registration, etc… The co- and cross-polarization gains of the antenna are computed as a function of the antenna's boresite and scan angle. Following the discussion in [10], the noise power measured by the antenna is computed using the following formula,

$$T_{Ant.}(f|\hat{r}_0) = \frac{\iint_{4\pi} T_b(f,\theta,\phi)\, P_n(f,\theta,\phi|\hat{r}_0) \sin\theta \, d\theta d\phi}{\iint_{4\pi} P_n(f,\theta,\phi) \sin\theta \, d\theta d\phi},$$

where T_b is defined in section 2.3 and P_n is the total antenna pattern (co- and cross-polar). The calculation of $T_{Ant.}$ is computationally intensive so it is split into two parts. T_b varies slowly with time and can be expensive to compute, requiring several minutes if a raytracing radiative transfer method is used. Because it is slow to compute, a lookup table of T_b is created over the whole visible sky at one degree intervals. This table filled once and used for up to one hour of simulation time before being recomputed. The antenna gain $P_n(f,\theta,\phi|\hat{r}_0)$ changes at every pulse as the antenna scans the sky, but it can be computed quickly for each pulse, then integrated against the precomputed table of sky temperatures.

2.5 RADAR CROSS SECTION CALCULATION

Having an accurate radar cross section model for targets is crucial to performing an accurate radar simulation. TESSA has several radar cross section models which can be used depending on the desired accuracy and availability of information. When catalog objects are used in the simulation, their RCS value from the Satellite Situation Report is used if there is no mesh information available. For other objects, either satellites with CAD models available or simulated debris objects from a hydro code, an RCS calculation method is chosen based on the objects' size. For very small debris objects where the object size is much less than a wavelength, a Rayleigh scattering approximation is used [11]. For larger objects in the resonant regime, EIGER, Electromagnetic Interactions GEneRalized, an in-house, parallel, method-of-moments solver is used [12]. This solver supports metals and dielectric materials, and provides highly accurate solutions for RCS. For objects which are many wavelengths in size, two models can be used. One is a code based on Physical Optics, which reduces the current integrals over facets to integrals over their edges [13] along with the Physical Theory of Diffraction [11] to handle scattering from edges. The other computation method used for large scatterers is the fast method implementation of EIGER. EIGER contains a parallel implementation of the Fast Multipole Method – Fast Fourier Transform (FMM-FFT) method [14]. This method allows for highly accurate fast solutions for radar cross section problems, while making load balancing and communication in parallel simpler than the Multilevel Fast Multipole Method [15]. Figure 5 shows a comparison of the RCS generated using the Physical Optics method and EIGER. While the Physical Optics has good agreement with the high fidelity model for specular scattering, returns near monostatic vary by 10dB between the methods. It is important to note that the difference in computational cost between the methods; EIGER required 1.7 hours on 16 processors for the simulation, while the Physical Optics method took just under 10 minutes on a single processor.

For RCS computations using EIGER or Physical Optics a cumulative distribution of RCS values for each object is precomputed before the radar simulation. This distribution is formed by computing the monostatic RCS of each object at 1536 equally-spaced locations and filling the results into a histogram. During the simulation, when the RCS of a target is needed, it is taken randomly from the cumulative distribution. Radar Cross Section values which are generated using Rayleigh scattering or from the Satellite Situation Report are not formed into a distribution; instead a single value is always used for the object.

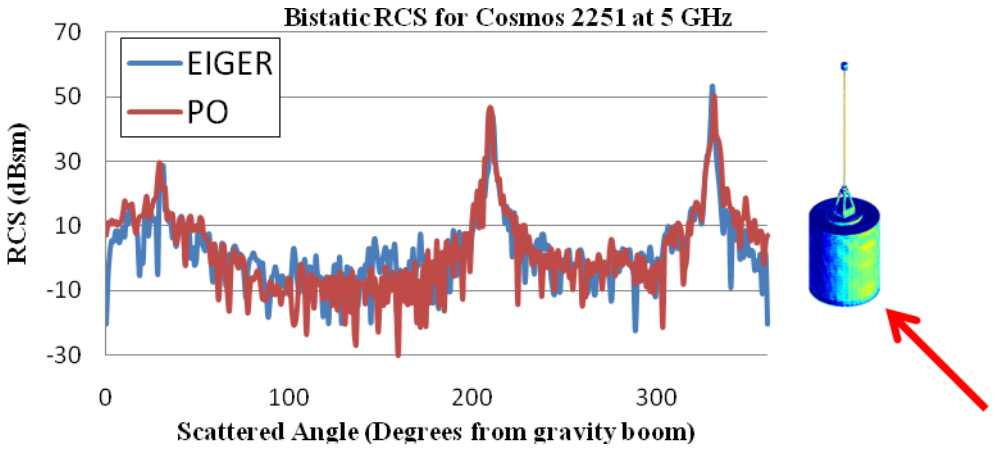

Figure 5. The Bistatic RCS computed in EIGER and with Physical Optics for the Cosmos 2251 satellite at 5 GHz and an incident angle of 150 degrees. The two methods show reasonable agreement for the main specular peeks, but not for the backscattered result near 150 degrees. The incident field direction is shown by the red arrow.

2.6 MPI PARALLELIZATION

The computationally intensive nature of this radar model demands parallelization. By parallelizing the model, we can decrease the run time so that trade studies of radar designs or placement can be run quickly without sacrificing simulation accuracy. The radar simulation is parallelized in several stages. All parallelization is done using the Message Passing Interface (MPI) [16]. The TESSA framework that this model is a part of automatically assigns each radar in a simulation to its own processor or bank of processors. If low fidelity, inexpensive modules alone are used, this level of parallelization may be sufficient. When more intensive modules are used, each radar is parallelized further. First, the simulation duration is broken into smaller time blocks, typically one hour in duration. For these short blocks, some of the modules fill lookup tables which are referenced at each pulse rather than being recomputed. Examples of this include the ionosphere module, which samples the electron density with 5km spacing, and the antenna module, which performs part of the antenna temperature calculation through a table. These tables can require many minutes to fill, and the same data is needed on every processor. To handle these tables efficiently, these tables are split with each processor computing the same number of entries. The completed entries are then shared so a complete table is on every processor.

After the tables are completed, the radar pulses are split among the processors. Each processor is responsible for the complete simulation of a contiguous block of pulses. Dividing the workload by pulses has two main advantages. The first is that most of the individual modules that are called at each pulse do not have to be parallelized, which speeds development. The second advantage is for saving time on orbital propagation. Orbital propagation of radar targets can be time consuming if a force model propagator is used. The force model propagator in TESSA precomputes a table of locations at five to ten minute intervals, then propagates the objects only from the last table entry during the simulation. By splitting the pulses in time, each processor only has to update the position and process from the nearest table entry.

Once all pulses are simulated, the observations are packed and sent to the master processor for assignment to tracks. While this final stage is not load balanced, the simple tracking algorithm used is not a dominant cost in the simulation. Using this method, efficient scaling has been demonstrated from 1-16 processors per radar. Future work in parallelization will include parallelizing advanced tracking algorithms as they are implemented.

3. SPACE FENCE EXAMPLE

To demonstrate the models capabilities, it was used to implement a notional S-band space fence radar located at four installations. This radar is not meant to represent a specific future space fence radar, but to be similar to one possible design. The radar sites included three locations in the United States roughly along the 33rd parallel (Gila River, Lake Kickapoo, and Jordan Lake) as well as one Australian site, Canberra, located at latitude 35.3 South. The radar operating frequency was 3.5 GHz, with an opening fan in the East-West direction from 10 degrees above

either horizon and the ability to track objects through 22.5 degrees of arc when passing through the fan. The radar is assumed to use a monopulse array for the actual tracking of objects once detected. The radar is designed to detect objects as small as 5cm at a range of 1000 km, and has a maximum effective range of 20,000 nautical miles. These parameters give it better sensitivity and slightly better range than the existing VHF space fence, while maintaining a similar level of accuracy. Because this radar model operates in monostatic mode with some ability to track an object that penetrates its beam, preliminary object orbits can be determined on the first orbit.

Detection and accuracy of a given observation depends on the signal-to-noise ratio of the observation. The radar is tuned to have a skin track range of 5225 km, which allows it to detect a 20cm object at 2200km or a 5cm object at around 1000km. The minimum signal-to-noise ratio used for detection is 12 dB. During the simulation, the signal-to-noise ratio for a given target is used to determine the error in the observation, which is assumed to be Gaussian. A Cramer-Rao lower bound model for error from monopulse radar is used. This model results in angular accuracy of around $1/6^{th}$ of the beamwidth for 12 dB targets at the limit of detection, and around $1/30^{th}$ of a beamwidth for extremely strong targets.

During the simulation, the radar is scheduled to continuously observe the sky. A simple pulse-scheduling algorithm was assumed, which allowed the radar to update the position of every object within its field of view once a second. For every observation, the signal-to-noise ratio was computed taking into account radar parameters, such as power and antenna pattern, distance to target, and object radar cross section. This signal-to-noise ratio then determined the accuracy of the observation and if the object was detected. For all objects detected, the observation plus appropriate error was passed to the tracking algorithm.

The test runs were performed on HERA, a LINUX-based supercomputer cluster at Lawrence Livermore National Laboratory. HERA consists of 13,824 2.3 GHz AMD Opteron Quad Core processors with 2 GB of memory per processor. The simulation required only a small fraction of the computer, using between 4 and 64 processors.

The simulated space fence radars were examined for their ability to detect debris from the Cosmos 2251 – Iridium 33 collision on February 10, 2009. This debris was created using a hydrodynamic code and full CAD models of the two satellites. The debris catalog contained 414 objects with mean RCS values ranging from 3.7 dbsm to -57 dbsm. The radar simulation was carried out at two levels of fidelity. Both used the antenna model and high accuracy RCS values. However, for case one, all galactic noise sources, atmospheric effects, and propagation losses were turned off. In case two, these effects were turned on. The radars were simulated for the first 12 hours after the collision, and statistics on observation errors and number of tracks established were computed.

The radar simulation for case one recovered at least one track for 99 off the objects in the first 12 hours after the collision, with an average positional error of 306m. Simulation case two with all modules turned on only recovered 96 of the objects with a higher average positional error, 325m. The number of objects which had preliminary tracks determined by each sensor are shown in Figure 6. It can be seen that the Australian space fence site at Canberra was the least useful at quickly recovering tracks based on this collision.

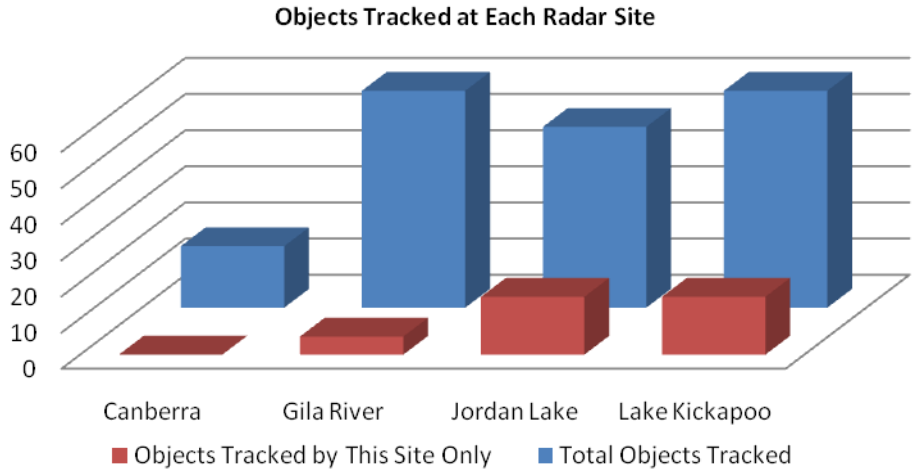

Figure 6. A comparison of the objects tracked at each radar site using the high fidelity model. The Gila River and Lake Kickapoo sites recovered the most tracks, with the Lake Kickapoo site recovering the most objects not recovered by any other sensor.

Timing results were captured for case one and case two. For case one using eight processors per radar, the simulation took only 172 seconds to complete. Case two with all atmospheric effects turned on took considerably longer, 802 seconds with eight processors per radar. The parallel scaling was tested for case two from 2-16 processors per radar, with the timing results shown in Table 1. It can be seen that the parallelization is around 80% efficient; doubling the number of processors causes the run time to drop by 40%.

Table 1. Simulation Run Time Scaling

Processors Per Radar	Run Time (s)
2	2020
4	1265
8	802
16	487

4. CONCLUSION

A high-fidelity parallel radar simulation was developed for modeling existing or proposed sensors in the Space Surveillance Network. This model includes antenna effects for modeling errors due to the IMU's and phase shifters, as well as polarization and gain patterns. It includes antenna temperature noise due to galactic noise distribution, as well as atmospheric effects. These high-fidelity modules are time consuming to compute, so the software is parallelized on a per-pulse basis. Using this parallelization, four potential space fence radars were tested against 414 debris objects for 12 hours of observation in less than 10 minutes of wall time. This speed shows the potential for this radar simulation to be used for radar trade studies and gap analysis off the SSN sensors.

5. REFERENCES

1. de Oliveira-Costa et al., "A model of diffuse Galactic Radio Emission from 10 MHz to 100 GHz," Monthly Notices of the Royal Astronomical Society, Volume 388, Issue 1, pp. 247-260
2. S. Hunt et al., "Equatorial Atmospheric and Ionospheric Modeling at Kwajalein Missile Range," *Lincoln Laboratory Journal*, vol. 12, no. 1, pp.45-64, 2000
3. B. R. Bean and G. D. Thayer, "CRPL Exponential Reference Atmosphere," NBS Monograph 4, U. S. Govt. Printing Office, Oct. 1959.
4. NOAA, NASA, U. S. Air Force, U. S. Standard Atmosphere 1976, U. S. Government Printing Office, Washington, DC, 1976
5. Y.T. Chiu "An improved phenomenological model of ionospheric density," *J. Atmos. Terr. Phys.* **37** (1975), pp. 1563–1570
6. D. Bilitza, "International Reference Ionosphere 2000," Radio Science 36, no 2, 261-275, 2001
7. H. J. Liebe, "MPM-An atmospheric millimeter-wave propagation model," *Int. J. Infr. Millimeter Waves*, vol. 10, no. 6, pp. 631–650, 1989
8. Marini, J. W. "Correction of Satellite Tracking Data for an Arbitrary Tropospheric Profile," Radio Science, 7, 223-231, 1972
9. K. C. Yeh and C. H. Liu, *Theory of Ionospheric Waves,* Academic Press, New York, 1972
10. German Cortes Medellin, "Antenna Noise Temperature Calculation," *SKA memo 95*, July 2007 (*http://www.skatelescope.org/PDF/memos/Memo_95.pdf*).
11. Maffett, Andrew. *Topics for a Statistical Description of Radar Cross Section*, New York: John Wiley & Sons, 1989.
12. Sharpe, R.M.; Grant, J.B.; Champagne, N.J.; Johnson, W.A.; Jorgenson, R.E.; Wilton, D.R.; Brown, W.J.; Rockway, J.W., "EIGER: Electromagnetic Interactions GEneRalized," *Antennas and Propagation Society International Symposium, 1997. IEEE., 1997 Digest* , pp.2366-2369, 13-18 Jul 1997.
13. Gordon, W.B., "High frequency approximations to the physical optics scattering integral," *IEEE Transactions on Antennas and Propagation*, vol.42, no.3, pp.427-432, Mar 1994.

14 Waltz, C.; Sertel, K.; Carr, M.A.; Usner, B.C.; Volakis, J.L., "Massively Parallel Fast Multipole Method Solutions of Large Electromagnetic Scattering Problems," , *IEEE Transactions on Antennas and Propagation*, vol.55, no.6, pp.1810-1816, June 2007.
15 W.C. Chew, J-M. Jin, E. Michielssen, J. Song, *Fast and Efficient Algorithms in Computational Electromagnetics*, Boston: Artech House, 2006.
16 Pacheco, Peter, *Parallel Programming with MPI*, San Francisco: Morgan Kaufmann Publishers, 1997.